Nonequilibrium linked cluster expansion for steady-state quantum transport

Petr Král*
Institute of Physics, Academy of Sciences, Na Slovance 2, 180 40 Praha 8, Czech Republic
(Received 15 October 1996; revised manuscript received 15 April 1997)

We generalize the linked cluster expansion of Matsubara Green functions into nonequilibrium situations. This allows us to compute nonequilibrium correlation functions and, consequently, physical observables for interacting quantum systems with intermediate interaction strengths. As a specific example, we study nonlinear dc transport in a resonant tunneling system with electron-phonon interaction. The first- and second-order nonequilibrium cluster approximations are explicitly evaluated. The results are compared with those obtained by the standard nonequilibrium Green functions approach within the Migdal approximation for the self-energy and in the low-density limit also with the known exact solution. For moderately strong electron-phonon interactions the first-order linked cluster approximation is more precise than the Migdal approach. The second-order approximation appears to be problematic in the presence of the Fermi sea. [S0163-1829(97)02435-1]

I. INTRODUCTION

Presently, systems of reduced dimensionality are studied intensively, where strongly nonequilibrium conditions can be easily maintained by weak external fields and where interactions become more important due to confinement of the electron states. A generic example is resonant tunneling systems in the presence of electron-phonon interaction. The experimental observation of phonon-mediated resonant channels[1] (sidebands) in these low-dimensional structures has stimulated numerous theoretical studies,[2–4] which address also intermediary strong electron-phonon interactions. These moderately interacting systems have been less investigated theoretically in general steady-state nonequilibrium conditions.

Quantum systems out of equilibrium can be described by nonequilibrium Green functions (NGF's) introduced by Kadanoff and Baym[5] or Keldysh.[6] The transport equations for nonequilibrium correlation functions of this method have been used to describe various nonequilibrium systems, including the resonant tunneling assisted by phonons.[7–12] In practice, however, NGF's are often limited to perturbative many-particle approximations, characterized by some subsets of Feynman diagrams, and thus restricted to relatively weak many-body interactions.[13] Nevertheless, recently the NGF method has been successfully applied to some strongly interacting quantum systems in nonequilibrium.[14–17]

Some intermediary interacting many-particle systems in equilibrium can be described by a linked cluster expansion[18] (LCE). Evaluation of the Green functions in this method is based on an approximate summation of the Feynman diagrams, different from the Dyson equation. In systems with an electron-phonon interaction[19,20] it was found that the method works rigorously only in the presence of one (Fermi) particle interacting with bosons,[18] analogously to the path integral evaluation of physical properties of polarons.[21] However, the possibility is left open that in a restricted region of parameters the method gives reasonable results also for systems with a finite density of particles.

In such a region of parameters the equilibrium LCE method for Matsubara Green functions can be generalized to nonequilibrium by analytical continuation, just as in the NGF method.[5] Following this way we obtain a hybrid method, *nonequilibrium linked cluster expansion* (NLCE), which combines features of both the NGF and LCE methods. In particular, the approach can describe some nonequilibrium quantum systems with moderately strong interactions.

As an illustration we apply the NLCE method to a simple resonant tunneling model with a moderately strong electron-phonon interaction and study its nonlinear response to a dc bias. General nonequilibrium conditions are maintained by keeping the resonant level partly populated. We compare our numerical results with the standard NGF method with a self-energy in the Migdal approximation.[22] For intermediate interaction strengths, usual in polar semiconductors, we find that the NLCE method in the first cluster approximation is more precise than the approximate NGF method. We have checked this directly by comparison with the exact solution, available in the low-electron-density limit. The second cluster approximation appears to be problematic at moderately strong interactions and in the presence of a Fermi sea, similarly as the original LCE method.

This paper is organized as follows. In Sec. III the LCE method for Green functions is extended into nonequilibrium. In Sec. III this approach and the NGF method with a self-energy in the Migdal approximation are applied to a resonant tunneling model with an electron-phonon interaction in a dc bias. In Sec. IV numerical results of both methods for the dc properties of the model are compared and limitations of the methods are discussed.

II. LINKED CLUSTER METHODS

Here we briefly review some basic features of the linked cluster expansion (LCE) for one-particle Matsubara Green functions.[18] Next, we present the extension of the LCE to nonequilibrium situations (NLCE).

A. Equilibrium LCE

Consider a quantum many-particle system described by the Hamiltonian $H=H_0+\lambda H_1$, where H_0 is diagonalizable

and H_1 contains the interactions. λ is a formal device used to enumerate the order of the perturbation expansion, which is set to $\lambda=1$ at the end of the calculation. In equilibrium this system can be described by the Matsubara Green functions, which can be perturbatively expanded in terms of the interaction part of the Hamiltonian H_1 as follows:[18]

$$G(1,2)=-\frac{\langle T_\tau[S(\beta)c(1)c^\dagger(2)]\rangle_0}{\langle S(\beta)\rangle_0}=\sum_{n=0}^{\infty}\lambda^n W_n(1,2)$$

$$=G_0(1,2)\exp\left[\sum_{n=1}^{\infty}\lambda^n F_n(1,2)\right]. \tag{2.1}$$

In the second equality of Eq. (2.1), $G(1,2)$ is expressed in terms of connected Feynman diagrams which are arranged according to the perturbation order n in the *clusters* W_n. The linked cluster expansion for the Green function (LCE) results if this series of W_n is resummed in terms of the as-yet-undetermined objects F_n, as shown in the second line. The expansion coefficients F_n are evaluated by equating the coefficients of the interaction parameter λ of the two expansion in Eq. (2.1):

$$F_1(1,2)=\frac{W_1(1,2)}{G_0(1,2)},$$

$$F_2(1,2)=\frac{W_2(1,2)}{G_0(1,2)}-\frac{1}{2}F_1(1,2)^2,\ \ldots. \tag{2.2}$$

The higher-order expressions get rapidly quite complicated. Importantly, however, it is often sufficient to consider in the expansion (2.1) only the first- and second-order terms F_1 and F_2. The advantage of the method is that it provides a convenient way of doing an infinite resummation; the disadvantage is that it may lead to unphysical results, in particular for strongly interacting many-particle systems.

The inherent limitations of the linked cluster expansion can be traced to the fact that higher-order Feynman diagrams in Eq. (2.1) are approximated by lower-order diagrams. Experience shows that this limitation is less serious in the absence of the Fermi sea, i.e., for one fermion interacting with Bose excitations. In this case both the full Green function[19,20] $G(k,\omega)$ and its local component[23] $G(\omega)=\Sigma_k G(k,\omega)$ have been succesfully calculated by LCE. In the presence of the Fermi sea the expansion of the full Green function $G(k,\omega)$ includes terms proportional to the number of particles, N, present in the system, which can limit the convergence of the expansion (2.1).[18] Terms proportional to N do not occur in the expansion of the local element[24] $G(\omega)$, where the Pauli principle prevents more than one electron occupying a given level. However, coupling to other levels involves all particles in the problem, and consequently the application of the LCE method requires care. Due to heavy numerics, the LCE method can be also evaluated here only for several lowest clusters. It could be expected that this approximated method gives reasonable results at least in a restricted parameter space.

We investigate the validity of this surmise on a model system, mentioning situations where problems begin to arise. Since our primary goal is to study nonequilibrium conditions, we do not use the original LCE method but its nonequilibrium version resulting from analytical continuation.

B. Nonequilibrium LCE

To obtain the nonequilibrium version of LCE, we can perform the analytical continuation and reduction to real times in the term $\Sigma_n\lambda^n W_n(1,2)$ in Eq. (2.1), just as done in the derivation of the Kadanoff-Baym equations.[5] Analogously, in the steady-state case, the starting point t_0 of the complex time path can be set to infinite past. The nonequilibrium linked cluster expansion (NLCE) for the correlation function $G^<(1,2)\equiv\langle c^\dagger(1)c(2)\rangle$ in real times then results by resummation of the new series as follows [the correlation function $G^>(1,2)$ can be obtained similarly]:

$$G^<(1,2)=\sum_{n=0}^{\infty}\lambda^n W_n^<(1,2)=G_0^<(1,2)\exp\left[\sum_{n=1}^{\infty}\lambda^n F_n^<(1,2)\right]. \tag{2.3}$$

The expansion coefficients $F_n^<$ are given by a nonequilibrium generalization of Eqs. (2.2):

$$F_1^<(1,2)=\frac{W_1^<(1,2)}{G_0^<(1,2)},$$

$$F_2^<(1,2)=\frac{W_2^<(1,2)}{G_0^<(1,2)}-\frac{1}{2}F_1^<(1,2)^2,\ \ldots, \tag{2.4}$$

where the correlation functions for the cluster diagrams $W_n^{<,>}(1,2)$ can be found from $W_n(1,2)$ by application of the Langreth rules.[25]

Another possibility of how to combine the NGF and LCE methods is to perform the analytical continuation in the LCE expansion for the spectral function $A(1,2)=G^>(1,2)+G^<(1,2)$ (or the propagator G^r). This version of the NLCE method does not give all the information contained in the correlation functions $G^<$, $G^>$, but in some situations this information is not necessary. The expansion looks as follows:

$$A(1,2)=G^>(1,2)+G^<(1,2)=\sum_{n=0}^{\infty}\lambda^n[W_n^>(1,2)+W_n^<(1,2)]$$

$$=[G_0^>(1,2)+G_0^<(1,2)]\exp\left[\sum_{n=1}^{\infty}\lambda^n F_n^A(1,2)\right], \tag{2.5}$$

where the coefficients F_n^A are obtained as before,

$$F_1^A(1,2)=\frac{W_1^>(1,2)+W_1^<(1,2)}{G_0^>(1,2)+G_0^<(1,2)},$$

$$F_2^A(1,2)=\frac{W_2^>(1,2)+W_2^<(1,2)}{G_0^>(1,2)+G_0^<(1,2)}-\frac{1}{2}F_1^A(1,2)^2,\ \ldots. \tag{2.6}$$

This expansion is in many aspects similar to the expansion (2.3) but it can be numerically more stable in certain situations. This is because the spectral function A is not sharply cut by the Fermi-Dirac distribution n_{FD} at low temperatures

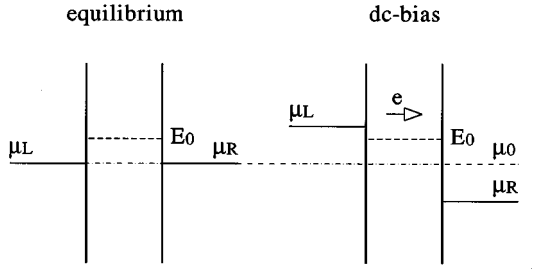

FIG. 1. A schematic drawing of the resonant tunneling system in the wideband approximation. In equilibrium the chemical potentials in the reservoirs $\mu_{L,R}$ coincide. Under a dc bias they shift equal amounts but in opposite directions with respect to the equilibrium chemical potential μ_0.

as the correlation functions $G^<$, $G^>$ in the former expansion. In the examples presented in the following sections the results for the spectral function A calculated either from Eq. (2.3) or (2.5) are practically identical.

The two NLCE methods in Eqs. (2.3) and (2.5) coincide in the limit of low electron (hole) concentration, $n_{\mathrm{FD}}\rightarrow 0(1)$, since in this limit one has $G_0^<(\omega)\rightarrow 0$, $G_0^>(\omega)\rightarrow A_0(\omega)$ [$G_0^<(\omega)\rightarrow A_0(\omega)$, $G_0^>(\omega)\rightarrow 0$]. In these one-particle limits also the LCE and other one-particle methods[2–4] can be safely applied. Therefore it is possible to compare the NLCE approach with the LCE method, which is known to give exact results for certain special cases.[18] Below we show in terms of a model example that in the limits $n_{\mathrm{FD}}\rightarrow 0(1)$ the NLCE method can give results which cannot in practice be distinguished from the exact solution found by the LCE method. Another interesting special situation corresponds to the high-temperature limit, where $n_{\mathrm{FD}}=$ const $(0<$ const $<1)$ in the studied spectral region.

III. APPLICATION TO TUNNELING

Here we study by the NLCE method electron transport in a simple resonant tunneling system with a moderately strong electron-phonon interaction and general nonequilibrium conditions under a dc bias. The results are compared with those obtained by the standard NGF approach.

A. Model

Our model is formed by a double-barrier structure with a resonant state located in the well between the two barriers.[7] The state is coupled via the tunneling barriers to two half-space reservoirs. In order to broaden the more general transport regimes with a partially occupied resonant level, we assume that the bands in the reservoirs are very wide. No interactions are considered in the reservoirs; however, the level is coupled to optical phonons. For simplicity, we assume that the phonons are not changed by the electron-phonon coupling, as it might be approximately correct for extended modes. A sketch of the model is shown in Fig. 1.

The spinless Hamiltonian for this system can be written as follows:

$$H=\sum_{k;\alpha=L,R} E_{k,\alpha}c_{k,\alpha}^{\dagger}c_{k,\alpha}+E_0 d^{\dagger}d + \sum_{k;\alpha=L,R} \gamma_{k;\alpha}(c_{k,\alpha}^{\dagger}d+\mathrm{H.c.})+\sum_q \hbar\omega_q b_q^{\dagger}b_q + \sum_q M_q d^{\dagger}d(b_q+b_{-q}^{\dagger}), \tag{3.1}$$

where $E_{k,\alpha=L,R}$ is the spectrum of energies for conduction electrons in the left (right) reservoirs, E_0 is the energy of the level, and $\gamma_{k,\alpha=L,R}$ are the coupling parameters between the level and the reservoirs. The optical phonons are characterized by the energies $\hbar\omega_q$ and the interaction matrix elements M_q, which can be approximated by the constants $\hbar\omega_0$ and M, defining the effective strength of the interaction $g=(M/\hbar\omega_0)^2$. The dc bias is simply modeled by different chemical potentials in the reservoirs $\mu_{L,R}$, which shift in the same amount but in opposite directions with respect to the equilibrium chemical potential μ_0 and the rigid position of the level.

B. NGF description of transport

The system can be described by nonequilibrium Green functions.[5] In a steady state the integral form of Kadanoff-Baym (KB) equations for nonequilibrium correlation functions can be written in a frequency representation as follows:[26]

$$G^<(\omega)=G^r(\omega)\Sigma^<(\omega)G^a(\omega),$$

$$G^>(\omega)=G^r(\omega)\Sigma^>(\omega)G^a(\omega). \tag{3.2}$$

Since the interaction is present only in the well, the analysis can be simplified by considering only the well diagonal elements of the above equations.

Coupling to the reservoirs can be described by the coupling (surface) Green functions[27] approximated by $\gamma_{L,R}^2 G_{L,R}^r(\omega)$, where $\gamma_{L,R}$ are effective local coupling constants and $G_{L,R}^r(\omega)$ are local elements of the Green functions in the reservoirs. In the wideband limit (WBL), intentionally considered in this work, the coupling Green functions can be further replaced by the imaginary constants[28] $-i\Gamma_{L,R}/2$. Then the free and interacting nonequilibrium electron propagators for the level result as follows:

$$G_0^r(\omega)=\frac{1}{\hbar\omega-E_0-\gamma_L^2 G_L^r(\omega)-\gamma_R^2 G_R^r(\omega)} \approx \frac{1}{\hbar\omega-E_0+i(\Gamma_L+\Gamma_R)/2},$$

$$G^r(\omega)\approx\frac{1}{\hbar\omega-E_0+i\Gamma/2-\Sigma_c^r(\omega)}, \quad \Gamma\equiv\Gamma_L+\Gamma_R, \tag{3.3}$$

where $\Sigma_c^r(\omega)$ is the propagator self-energy describing many-particle interactions.

The correlation functions for the self-energy in Eqs. (3.2) are equal the sum of the hybridization (coupling) parts $\Sigma_h^{<,>}(\omega)$ and the many-particle parts $\Sigma_c^{<,>}(\omega)$,

$$\Sigma^<(\omega)=\Sigma_h^<(\omega)+\Sigma_c^<(\omega),$$

$$\Sigma^>(\omega)=\Sigma_h^>(\omega)+\Sigma_c^>(\omega). \tag{3.4}$$

In the WBL approximation the hybridization contributions result as

$$\Sigma_h^<(\omega)\approx\Gamma_L n_{\rm FD}(\hbar\omega-\mu_L)+\Gamma_R n_{\rm FD}(\hbar\omega-\mu_R),$$

$$\Sigma_h^>(\omega)\approx\Gamma_L[1-n_{\rm FD}(\hbar\omega-\mu_L)]+\Gamma_R[1-n_{\rm FD}(\hbar\omega-\mu_R)], \tag{3.5}$$

where $n_{\rm FD}$ is the Fermi-Dirac distribution function.

In systems without translational invariance the electron-phonon interaction has a nonzero Hartree contribution to the electron self-energy, which gives an additional polaron shift of the resonant level.[12] The self-consistency with respect to redistribution of charges, included in a Hartree (Coulomb) term, has been mentioned in the past.[29,30] In our studies, focused on many-particle effects, we neglect the Hartree term and take the electron self-energy in the Migdal approximation[22] (see also Fig. 2). Then the correlation functions $\Sigma_c^<(\omega)$, $\Sigma_c^>(\omega)$ can be written as follows:

$$\Sigma_c^<(\omega)=\int\frac{d\overline{\omega}}{2\pi}M^2G^<(\omega-\overline{\omega})D^<(\overline{\omega})$$
$$=M^2\{G^<(\omega-\omega_0)n_{\rm BE}(\omega_0)+G^<(\omega+\omega_0)[1+n_{\rm BE}(\omega_0)]\},$$

$$\Sigma_c^>(\omega)=\int\frac{d\overline{\omega}}{2\pi}M^2G^>(\omega-\overline{\omega})D^>(\overline{\omega})$$
$$=M^2\{G^>(\omega-\omega_0)[1+n_{\rm BE}(\omega_0)]+G^>(\omega+\omega_0)n_{\rm BE}(\omega_0)\}, \tag{3.6}$$

where $n_{\rm BE}$ is the Bose-Einstein distribution function. In Eq. (3.6) free phonons in equilibrium are considered for simplicity. The self-energy propagators $\Sigma_c^{r,a}(\omega)$ can be obtained by Eqs. (A6) and (A7).

The solution of the KB equations (3.2) can be expressed as a pair of correlation functions $G^<(\omega)$, $G^>(\omega)$, which can be *formally* written as in equilibrium, Eq. (A5):

$$G^<(\omega)=A(\omega)f(\omega),$$

$$G^>(\omega)=A(\omega)[1-f(\omega)]. \tag{3.7}$$

Here both the spectral function $A(\omega)$ and the electron distribution function $f(\omega)$ are nonequilibrium quantities in the presence of the dc bias. From Eqs. (3.7) it becomes clear that static nonequilibrium systems can be represented by any two functions from $G^<(\omega)$, $G^>(\omega)$, $A(\omega)$, $f(\omega)$.

In nonequilibrium the distribution function $f(\omega)$ differs from the Fermi-Dirac form already in the absence of interactions. In this trivial case it can be immediately written down when substituting the hybridization correlation terms $\Sigma_h^{<,>}$ from Eqs. (3.5) into the free KB equations

$$G_0^<(\omega)=G_0^r(\omega)\Sigma_h^<(\omega)G_0^a(\omega),$$

$$G_0^>(\omega)=G_0^r(\omega)\Sigma_h^>(\omega)G_0^a(\omega). \tag{3.8}$$

For the symmetrical coupling $\Gamma_L=\Gamma_R=\Gamma/2$ the free distribution function $f_0(\omega)$ resulting from Eqs. (3.8), as in Eqs. (3.7), is a simply weighted sum of the distribution functions in the reservoirs:

$$f_0(\omega)=\frac{n_{\rm FD}(\hbar\omega-\mu_L)+n_{\rm FD}(\hbar\omega-\mu_R)}{2}. \tag{3.9}$$

For the symmetrical coupling the dc current running through the system can be calculated from the spectral function $A(\omega)=G^<(\omega)+G^>(\omega)$, resulting from Eqs. (3.2) or (3.8), by the following simple formula:[28]

$$J_{dc}=\frac{e\Gamma}{4\hbar}\int\frac{d\hbar\overline{\omega}}{2\pi}A(\overline{\omega})[n_{\rm FD}(\hbar\overline{\omega}-\mu_L)-n_{\rm FD}(\hbar\overline{\omega}-\mu_R)]. \tag{3.10}$$

In the one-electron approaches[2–4] often a Landauer formula very similar to Eq. (3.10) is used, where $A(\omega)$ is substituted by an equilibrium transmissivity $T(\omega)$. In finite-density nonequilibrium systems the spectral function can differ from its equilibrium form. Then the equilibrium transmissivity cannot be applied and the NGF method and the NLCE method, described below, are at hand.

C. NLCE description of transport

In application of the NLCE to our system, we explicitly evaluate the first- and second-order linked cluster coefficients[18] F_1, F_2 in Eqs. (2.4), (2.6), which can be found from the cluster terms W_1, W_2 in Eq. (2.1) (see also Fig. 2). Thereby we generalize the equilibrium results of Mahan[19] and Dunn[20] for electron-phonon interactions to nonequilibrium.

In Fig. 2 we show a diagrammatic expansion of the Dyson equation for the electron Green function G in the present problem. We neglect here and in the calculations the Hartree term and diagrams dressing phonon lines.[31] The last approximation could be possibly done for extended phonon modes, where the phonons can be also simply taken in equilibrium. If dressing is important, then also a fully self-consistent phonon dynamics, with a proper relaxation mechanism, should be included. In the expansion in Fig. 2 all diagrams with noncrossed phonon lines contribute to the Green function approximated by the Migdal self-energy[22] in Eq. (3.6). The remaining diagrams with crossed phonon lines form the vertex corrections.[32] We can identify here the diagrams corresponding to the clusters W_n, $n=0,1,2$, introduced in Eq. (2.1). The zeroth term W_0 is just the free Green function G_0. The first-order cluster W_1 is given by the first-order diagram with a single-loop self-energy. The second-order cluster W_2 is formed by three second-order diagrams denoted here by $W_{2a,b,c}$.

The nonequilibrium correlation functions $G^<(\omega)$, $G^>(\omega)$ in Eq. (2.3) or the spectral function $A(\omega)$ in Eq. (2.5) can be

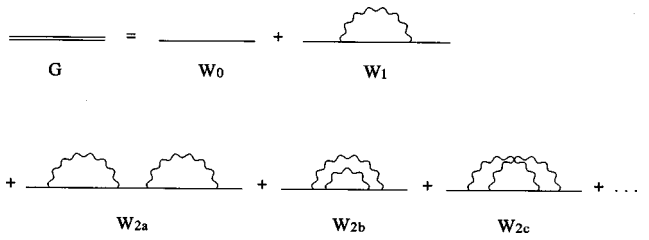

FIG. 2. Diagrammatic expansion of the Dyson equation for the Green function G in the electron-phonon interaction. All diagrams with noncrossed phonon lines contribute to the expansion of the Green function with the Migdal self-energy. The remaining diagrams form vertex corrections to this expansion. Diagrams contributing to the zeroth-, first-, and second-order clusters are denoted here by W_0, W_1, and $W_{2a,b,c}$.

obtained directly from the correlation functions $W_{1,2}^{<,>}(\omega)$, found in the Appendix B. To this goal $W_{1,2}^{<,>}(\omega)$ must be transformed into a time domain and divided by the free correlation functions $G_0^{<,>}(1-2)$. Then the exponentials in Eqs. (2.3) and (2.5) can be constructed, which are multiplied by $G_0^{<,>}(1-2)$. The resulting full correlation function $G^{<,>}(1-2)$ can be easily transformed back to the frequency representation. As a test of the results obtained by the NLCE method, we have numerically checked the sum rule $\int(d\omega/2\pi)A(\omega)=1$ in the examples presented below. The dc current can be calculated from the correlation functions $G^{<,>}(\omega)$ or the nonequilibrium spectral function $A(\omega)$ [cf. Eq. (3.10)], just as in the NGF method.

IV. NUMERICAL RESULTS AND DISCUSSIONS

Here we present numerical results computed with the NLCE and NGF methods for the tunneling model of the previous section and discuss the limitations of these approaches.

A. Spectral properties

Consider first the limit of low electron (hole) concentration, $n_{\mathrm{FD}}\to 0(1)$, where the one-electron methods work successfully.[2–4] Here also the two NLCE approaches for the correlation functions (2.3) and for the spectral function (2.5) coincide. Physically, this limit corresponds to the case when the electron level in the quantum well is far above (below) the Fermi level in the reservoirs, so that the problem can be solved as if only one electron (hole) is present in the system. The LCE method gives for the case $n_{\mathrm{FD}}\to 0$ the following exact solution for the causal (retarded for one electron) Green function[18] in the time representation:

$$G(t)=G_0(t)e^{-g\{[n_{\mathrm{BE}}(\hbar\omega_0)+1](1-ie^{-i\hbar\omega_0 t})+n_{\mathrm{BE}}(\hbar\omega_0)(1-ie^{i\hbar\omega_0 t})-i\hbar\omega_0 t\}},$$

$$G_0(t)=-\frac{i}{\hbar}\theta(t)e^{(-iE_0 t/\hbar-2\Gamma t)}, \tag{4.1}$$

where $G_0(t)$ is the free electron propagator (3.3). After a Fourier transform of $G(t)$ to the frequency representation, the exact spectral function $A(\omega)$ can be obtained as in Eq. (A6).

In Fig. 3 we show the equilibrium spectral function $A(\omega)$ in the limit $n_{\mathrm{FD}}\to 0$, calculated by the LCE method in Eqs. (4.1) and the NLCE and NGF methods discussed in the previous section. Numerically this limit is approached by substituting in the hybridization self-energies (3.5) the Fermi-Dirac distribution functions in the reservoirs by the value $n_{\mathrm{FD}}=0$. The other parameters are $E_0=15$ meV, $\Gamma=8$ meV, $\hbar\omega_0=30$ meV, $g=0.25$, and $T=70$ K. The Lorentzian free solution is shown by the dotted line, the exact solution in Eqs. (4.1) is shown by the dot-dashed line, the first- (second-) order NLCE solution corresponds to the thick (thin) solid line, and the NGF solution with the Migdal self-energy is drawn by the dashed line. In the interacting solutions a polaron shift of the central peak down to lower energies can be seen (a different shift would result in the presence of the Hartree term[12]). Here also characteristic satellite peaks (sidebands) can be observed, with energies shifted from the main peak by multiples of the phonon energy $\hbar\omega_0$. The magnitude of these satellites and the polaron shift of the main peak increase with the strength of interaction.[2] It is interesting that the NLCE solutions are

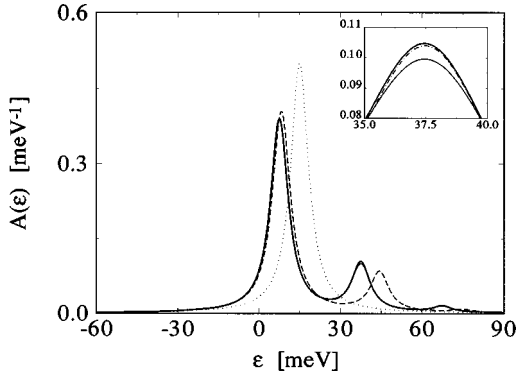

FIG. 3. The spectral function $A(\omega)$ for the tunneling model discussed in the text in the limit $n_{\mathrm{FD}}\to 0$. The parameters are $E_0=15$ meV, $\Gamma=8$ meV, $\hbar\omega_0=30$ meV, $g=0.25$, and $T=70$ K. The free solution is shown by the dotted line, the exact solution is shown by the dot-dashed line, the first- (second-) order NLCE solution corresponds to the thick (thin) solid line, and the NGF solution with the Migdal self-energy is drawn by the dashed line. The exact and NLCE solutions practically coincide everywhere, but the position of the first satellite, which we present magnified in the inset. The solution of the NGF method for the Migdal approximation for the self-energy gives considerably worse results.

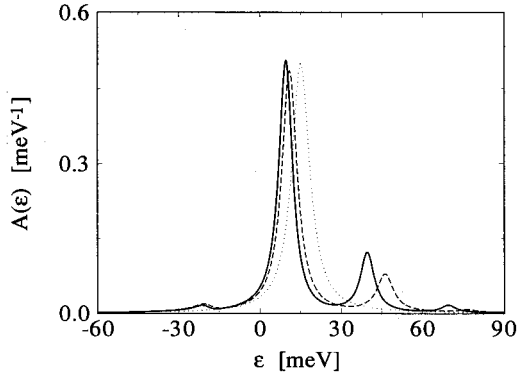

FIG. 4. The equilibrium spectral function $A(\omega)$ calculated by the NGF and NLCE methods for the parameters of Fig. 3 but with a finite density of particles corresponding to the standard form of the Fermi-Dirac distribution. Here the exact solution is not available. We present only the first-order solutions, since the second-order solution is problematic in the presence of the Fermi sea. The solution of the NGF method with the Migdal self-energy gives again a quite different satellite structure.

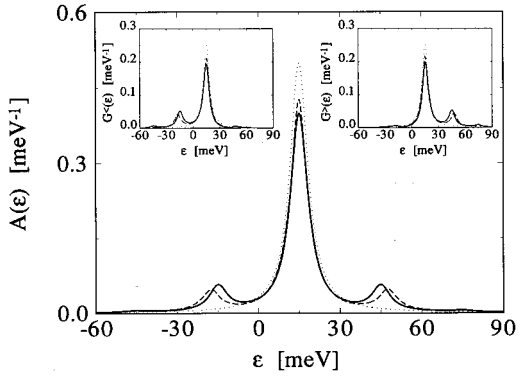

FIG. 5. The nonequilibrium spectral function $A(\omega)$ calculated by the methods and the same parameters as in Fig. 4. Here the bias is chosen $\mu_L = -\mu_R = 60$ meV. Note that the spectral function becomes symmetric for both NLCE and NGF methods, since the level is approximately half populated here. In the insets the nonequilibrium correlation functions $G^<(\omega)$, $G^>(\omega)$ are shown, which are for the present parameters close to each other's mirror images.

practically indistinguishable from the exact solution. In the inset we show tiny differences between the exact and NLCE solutions in the position of the first sideband. The small difference between the exact and NLCE solutions can be explained by the fact that the analytical structures of the exponent in the exact solution (4.1) and the NLCE solution with the F_1^A coefficient in Eq. (2.6) show minor differences for the presently used parameters ($\hbar\omega_0 \approx 4\Gamma$). Quite remarkably, the solution of the NGF method with the Migdal approximation of the self-energy, shown by the dashed line, leads to a significantly different satellite structure. Especially the different distance of the satellites from the main peak is seen. Similar differences have been also found on a two-level model and a continuous model, in the presence of the Fermi sea, with an electron-phonon interaction.[31]

The situation with a nearly empty (full) level appears, for example, when phonon satellites are measured in the tail of the resonant current through the level.[1] These limit populations can be hardly realized in such investigations for low-energy (acoustic) phonons[33,34] or when the bands coupled to the level are too wide. The WBL approximation used here is well suited to simulate these more general situations, which are beyond the scope of the transmissivity methods.[2–4] The influence of filling of the level on the tunneling current has been previously addressed[10,12] by the NGF method, but the present NLCE theory allows a more quantitative discussion of these phenomena in the presence of moderately strong interactions.

We can investigate this finite-density case, which physically corresponds to moving the level within the Fermi sea in such a way that the limit $n_{\rm FD} \to 0$ is fluently changed by $n_{\rm FD} \to 1$. Filling of the level depends on various factors, like matching of the bands of the reservoirs with the level or the ratio Γ_L/Γ_R of the coupling constants to the reservoirs.[12] In Fig. 4 the spectral function is shown for the same parameters as in the previous figure, but for the standard form of the Fermi-Dirac distribution $n_{\rm FD}$ ($\mu_L = \mu_R = \mu_0 = 0$), substituted in Eqs. (3.5). For the presently used parameters the first-order NLCE solution can be calculated without major troubles, but the second-order solution appears to be problematic at moderately strong interactions and in the presence of the Fermi sea, similarly as the original LCE method.[18] In this finite-density case the exact solution is no longer available, but from the similarity of Figs. 3 and 4 it can be expected that it is close to the presented first-order NLCE solution. We can observe that this NLCE solution gives here sharper satellites than in Fig. 4. The NGF solution with the Migdal self-energy is again very different.

The problems of the second-order solution result from the fact that the relevant exponent $F_2^A(t)$ in Eqs. (2.6) has a positive real part which rapidly grows with t and cannot be diminished for large t by the prefactor $A_0(t)$ in front of the exponent. Similar growth is present also in the first-order solution, but its limitation becomes serious for much stronger interactions or at low temperatures. It is not clear whether this fast growth could be renormalized in some way, as in other similar methods.[31] Here we show at least the reasonable solutions resulting from the present form of the NLCE method.

We can approach also the nonequilibrium situations, where both the spectral function $A(\omega)$ and the distribution function $f(\omega)$ can be strongly changed, as shown, for example, in resonant tunneling through a Kondo impurity.[14,15] In Fig. 5 the nonequilibrium spectral function $A(\omega)$ is calculated for our model for the parameters of Fig. 4 and the bias $\mu_L = -\mu_R = 60$ meV. Only the first-order approximation of the NLCE method is presented from the same reasons as in the previous figure. Here it is quite similar to the NGF solution. If the left chemical potential crosses the position of the level $\mu_L \approx E_0$, the spectrum calculated by both the NGF and NLCE methods becomes symmetrically located around the noninteracting solution, because the level becomes half filled due to $\Gamma_L = \Gamma_R$. This particle-hole symmetry is reflected by a mirror symmetry of the correlation functions $G^<(\omega)$, $G^>(\omega)$, shown in the insets. The symmetrization of the spectral function occurs for different biases even if $\Gamma_L \neq \Gamma_R$.[12] We mention that in the WBL approximation the

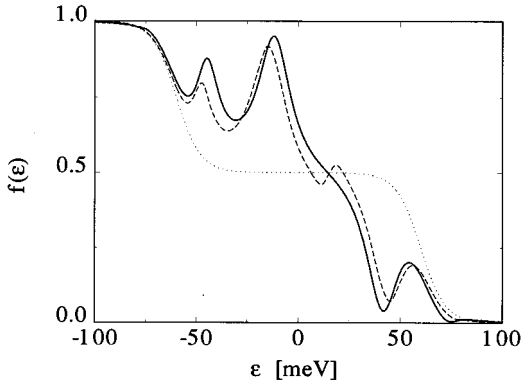

FIG. 6. The distribution function $f(\omega)$ calculated for the parameters in Fig. 4. The solution for the noninteracting model is formed by two Fermi-Dirac distributions shifted by the amount $|\mu_L-\mu_R|$. The NGF and NLCE show additional oscillatory structures, reflecting increased electron population in the satellite peaks.

satellites in the changing spectrum (Figs. 4 and 5) can be observed by the current probe only if they appear together with the central peak in the energy window (μ_L,μ_R).

In Fig. 6 we present also the nonequilibrium distribution function $f(\omega)$, resulting directly from the correlation functions (3.7) as $f(\omega)=G^<(\omega)/[G^<(\omega)+G^>(\omega)]$. The noninteracting distribution $f_0(\omega)$ is formed by two Fermi-Dirac distributions $n_{\rm FD}$ shifted by $|\mu_L-\mu_R|$ as shown in Eq. (3.9). The interacting distribution has been studied for weak interaction strengths in a model similar to ours.[9] For the stronger interactions investigated here we observe deep oscillations in these distributions, which are quite similar for the NGF and NLCE solutions. In the region of the central peak $\hbar\omega\approx 20$ meV the two solutions are a little different and in the NGF solution an inverted population appears, showing a lack of relaxation inside the central peak. The local maxima of the deep oscillations in the curve $|f(\omega)-f_0(\omega)|$ in Fig. 6 coincide with the positions of the satellites in Fig. 5. Therefore these oscillatory structures reflect increased nonequilibrium electron population in the satellite peaks. We have studied also tunneling systems with an electron-electron interaction,[35] where these structures show a different ability of this interaction to equilibrate the system to an increased temperature, given approximately by $k_B\Delta T\approx|\mu_L-\mu_R|$.

To present in a more clear way the results obtained by the NLCE method, we show in Fig. 7 the spectral function calculated by the first-order NLCE for the changed parameters: the level position $E_0=25$ meV, the temperature $T=300$ K, and the interaction strength $g=1$ (we have realized from numerical analysis that at these temperatures the NLCE is reliable for stronger coupling). The short-dashed line (upper drawing) shows the solution for the one-electron limit $n_{\rm FD}\to 0$, which can be also obtained by the LCE method,[2] the dashed line (middle drawing) corresponds to the presence of the Fermi sea, and the solid line (lower drawing) represents the nonequilibrium solution for $\mu_L=60$ meV. All the solutions in Fig. 7 differ by the polaron shift of the main peak, denoted by the solid small triangle, with respect to the position of the level, shown in the figure by a thin horizontal dot-dashed line. For $g=1$ the one-electron solution has a polaron shift down to lower energies equal the phonon energy[2] $\Delta_1=\hbar\omega_0$, so that the *first* satellite is at the position

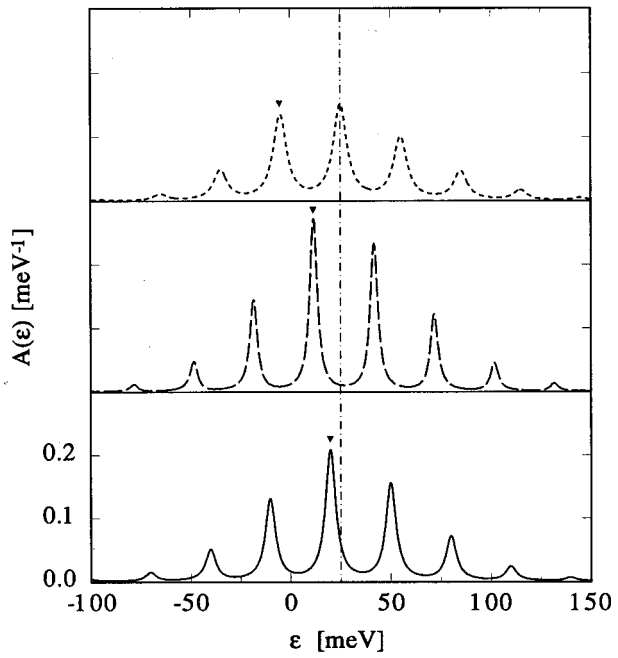

FIG. 7. The spectral function calculated by the first-order NLCE method for the changed parameters: the level position $E_0=25$ meV (thin horizontal dot-dashed line), the temperature $T=300$ K, and the interaction strength $g=1$. The short-dashed line (upper drawing) shows the one-electron limit $n_{\rm FD}\to 0$, the dashed line (middle drawing) corresponds to the presence of the Fermi sea, and the solid line (lower drawing) represents the nonequilibrium solution for $\mu_L=60$ meV. The polaron shift of the main peak, denoted by the solid small triangle, becomes smaller when going from the first to the last of these solutions as follows: $\Delta_1=\hbar\omega_0$, $\Delta_2\approx\hbar\omega_0/2$, $\Delta_3\approx\hbar\omega_0/4$. Also the symmetry of the spectra with respect to the main peak increases in this order.

of the level E_0. In the presence of the Fermi sea the polaron shift is smaller $\Delta_2\approx\hbar\omega_0/2$, due to filling of the level. In this solution also the peaks appear to be sharper and higher than in the one-electron limit. In nonequilibrium the level becomes even more filled by electrons, and as a result the shift further decreases to about $\Delta_2\approx\hbar\omega_0/4$. As the level filling approaches one-half, a symmetrization of the peak heights, with a center in the main (first) peak, can be also observed.

B. *I-V* characteristics

In many experimental resonant tunneling systems the bands for the reservoirs are narrow. As a result the current through the level resonantly falls down when the moving bands with a dc bias no longer mismatch the level. In our model the WBL approximation is applied and so the tunneling current does not resonantly fall down. Nevertheless, the tunneling current through the satellites can be still observed on the background of the current through the level.

In Fig. 8 we show the *I-V* characteristics of the present model calculated from Eq. (3.10) for the parameters in Figs. 4–6 and the bias in the interval $0<\mu_L=-\mu_R<70$ meV. Since at $T=70$ K the temperature spreading prevents a good observation of the tunneling through satellites (see the inset), we have calculated the *I-V* characteristics also for $T=30$ K, presented in Fig. 8. At this temperature clearly separated

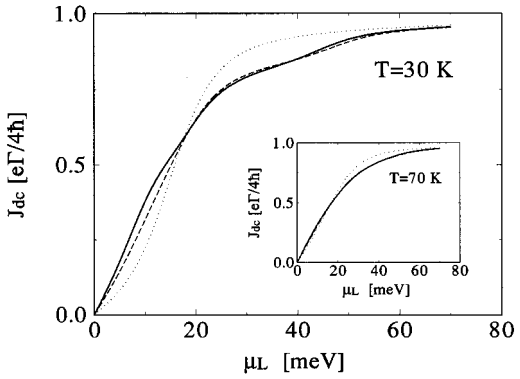

FIG. 8. The I-V characteristics for the example in Figs.4–6, the temperature $T=30$ K, and the biases in the region $0<\mu_L=-\mu_R<70$ meV. The noninteracting solution (dotted line) is structureless. The first-order NLCE solution (solid line) and the NGF solution (dashed line) show bumps, reflecting tunneling through individual peaks. In the inset the solution for $T=70$ K is presented, where bumps, are not seen due to temperature smearing.

bumps in the interacting solutions for the current can be observed, when the chemical potentials of the reservoirs cross the main peak or the satellites. In the current one bump is present above and one below the central region of the current ($\mu_L \approx 25$ μeV). The lower bump ($\mu_L \approx 10$ μeV) results from the polaron shift of the main peak in Fig. 4. This bump is slightly different in the NLCE and NGF solutions, because these two solutions give a little different polaron shifts. In fact contributions to the current from the main peak and the first satellite below it cannot be well distinguished for the present parameters, because these peaks are approximately at the same distance, but opposite directions, from the equilibrium position of the Fermi level. Therefore the main peak is crossed by the left chemical potential moving up at the same time when the first satellite below it is crossed by the right chemical potential moving down. The second bump ($\mu_L \approx 40$ μeV) appears when the chemical potential μ_L crosses the position of the first satellite above the main peak. At even higher biases the interacting solutions for the current approach the free solution and all solutions saturate to the value $e\Gamma/4\hbar$, which is the prefactor in formula (3.10). In ac linear response problems or general time-dependent situations the two methods should give more different solutions.

Let us briefly discuss the failure of the presented methods. It is evident that the NGF solution in the Migdal approximation gives results different from the exact solution because the crossed diagrams in Fig. 2 are neglected there. The wrong shift of satellites in this solution has been also observed elsewhere.[31] The limitation of the NLCE (LCE) method in systems with many particles is different from the approximate NGF method, but it is also serious. Particularly, the Green functions obtained in such a way do not fulfill automatically Herglotz properties (negative densities of states can appear) and the higher-order cluster approximations even do not seem to give a convergent solution at intermediary interaction strengths and in the presence of the Fermi sea. Based on our numerical results we estimate at least the region of validity of the first-order cluster approximation in NCLE. We have found that this method can give reasonable results, if the inequalities $g<0.5$, $\Gamma<kT$ are satisfied. In fact the limiting g is also dependent on T (see Fig. 7), so that the total region of validity is located in (g,Γ,T) space. The inequality $\Gamma<kT$ is determined by new physical effects, resulting, in the presence of interactions, from a high gradient of electron concentration in the region of the coupling broadened level. Such effects can be accounted only by iterative solutions, which sum infinite series of Feynman diagrams. In general the NLCE (LCE) method approximated by low-order clusters can only describe physical systems where the relevant physics is qualitatively included already in the lowest Feynman diagrams (no phaselike transitions). We do not give a more detailed analysis here, but hope that future works will further clarify the mentioned problems.

V. CONCLUSION

We have generalized into nonequilibrium the LCE method for Matsubara Green functions[18] by analytical continuation as in the NGF method.[5] The resulting stationary version of the NLCE method in the first cluster approximation can reasonably describe nonequilibrium finite-density systems with moderately strong interactions. The second cluster approximation of this method becomes problematic in finite-density systems as the original LCE method[18] and presently it is not clear to which extent this failure can be overcome.

The NLCE method has been tested on a simple resonant tunneling model with an electron-phonon interaction in a dc bias. Numerical results for the nonequilibrium spectral and distribution functions have been obtained in the first order and, in the weak density limit, in the second order of the cluster approximations. From these nonequilibrium spectra the dc resonant tunneling current has been found. The results were compared with the solution of the standard NGF method with a Migdal self-energy. For intermediate interaction strengths the first-order NLCE is more precise than this approximate NGF method, which neglects crossed Feynman diagrams. In the limit of a weak density of particles this has been checked by comparison with the exact solution of the problem. Spectra have been obtained for many-particle systems with an electron-phonon interaction with intermediary interaction strengths and in general nonequilibrium conditions. Unfortunately, here the second-order NLCE appears to be inapplicable in the present form.

We would like to investigate by the NLCE method also time-dependent quantum systems in ac (Refs. 36 and 37) and pulsed electric fields.[38] We believe that these studies could lead to a deeper understanding of nonequilibrium quantum systems with moderately strong interactions.

ACKNOWLEDGMENTS

The author would like to express many thanks to A. P. Jauho for a short hospitality in DTU Lyngby, many comments, and corrections in this work. Also he would like to thank B. Velický for useful discussions. He is grateful to P. Středa and J. Petzelt for help with finding financial support of this work. The numerical part of this work has been done on CRAY Y-MP EL in the Institute of Physics, Prague.

APPENDIX A

Here we present some relationships valid for Green functions (self-energy). The causal fermion ($O=\psi$) or boson ($O=A$) Green functions in real times are defined by[32] (temperature Matsubara Green functions[18] are defined analogously)

$$G^t(1,2)=-\frac{i}{\hbar}\langle T[O(1)O^\dagger(2)]\rangle, \quad j\equiv(r_j,t_j) \quad (j=1,2). \tag{A1}$$

Correlation functions are related to these causal functions as follows:

$$\begin{aligned} i\hbar G^t(1,2)&=G^>(1,2)=\langle O(1)O^\dagger(2)\rangle, \quad t_1>t_2,\\ &\mp i\hbar G^t(1,2)\\ &=G^<(1,2)=\langle O^\dagger(2)O(1)\rangle, \quad t_1<t_2, \end{aligned} \tag{A2}$$

where the upper (lower) sign applies to fermions (bosons).

The retarded and advanced Green functions are defined by

$$G^r(1,2)=-\frac{i}{\hbar}\theta(1-2)[G^>(1,2)\pm G^<(1,2)],$$

$$G^a(1,2)=\frac{i}{\hbar}\theta(2-1)[G^>(1,2)\pm G^<(1,2)], \tag{A3}$$

where $\theta(t)=0,\ t<0,$ and $\theta(t)=1,\ t\geq 0$.

In equilibrium and space homogeneous systems the Green functions depend only on the difference of coordinates $(r,t)=(r_1-r_2,t_1-t_2)$, so that they can be easily Fourier transformed to the (k,ω) representation as follows:

$$G(k,\omega)=\int d^n r\int dt\, e^{i(\omega t-r\cdot k)}G(r_1-r_2;t_1-t_2). \tag{A4}$$

The equilibrium fermion and boson correlation functions can be expressed as[5]

$$\begin{aligned} G^<(k,\omega)&=n_{F,B}(\hbar\omega)A(k,\omega),\\ G^>(k,\omega)&=[1\mp n_{F,B}(\hbar\omega)]A(k,\omega), \end{aligned} \tag{A5}$$

where n_F and n_B denote the Fermi-Dirac and Bose-Einstein distributions,

$$n_{F,B}(\hbar\omega)=\frac{1}{e^{\hbar\omega/kT}\pm 1},$$

and the spectral function is defined by

$$A(k,\omega)\equiv -2\,\mathrm{Im}\,G^r(k,\omega)=G^>(k,\omega)\pm G^<(k,\omega). \tag{A6}$$

The retarded Green function can be calculated from the spectral function (A6) by the Hilbert transform

$$G^r(k,\omega)=\int_{-\infty}^{\infty}\frac{d\overline{\omega}}{2\pi}\frac{A(k,\overline{\omega})}{\omega-\overline{\omega}+i\delta}. \tag{A7}$$

APPENDIX B

We evaluate the cluster coefficients $W_{1,2}^<$, $W_{1,2}^>$ for the above-discussed resonant tunneling model with the electron-phonon interaction. These correlation factors result by application of LW rules[25] in the causal terms $W_{1,2}$ written in Matsubara Green functions.

The lesser correlation factor $W_1^<$ can be written in a frequency representation as follows (similarly can be obtained the higher part $W_1^>$):

$$\begin{aligned} W_1^{<(>)}(\omega)&=G_0^{<(>)}(\omega)M^2[G_0(\omega-\overline{\omega})D(\overline{\omega})]^aG_0^a(\omega)\\ &+G_0^r(\omega)M^2G_0^{<(>)}(\omega-\overline{\omega})D^{<(>)}(\overline{\omega})G_0^a(\omega)\\ &+G_0^r(\omega)M^2[G_0(\omega-\overline{\omega})D(\overline{\omega})]^rG_0^{<(>)}(\omega), \end{aligned} \tag{B1}$$

where the bar over the frequency variable $\overline{\omega}$ means integration over this variable. The propagators $[G_0(\omega-\overline{\omega})D(\overline{\omega})]^{r,a}$ can be found from the correlated parts $G_0^{<(>)}(\omega-\overline{\omega})D^{<(>)}(\overline{\omega})$ by the Hilbert transform (A7). The free but nonequilibrium correlation functions and propagators for electrons, which are necessary in Eq. (B1), are in Eqs. (3.3) and (3.8). The phonon functions can be evaluated from Eqs. (A5) and (A7), with the use of the free phonon spectral function.[18]

The second-order coefficients $W_2^<$, $W_2^>$ are formed by three terms depicted in the diagram in Fig. 2. The first one $W_{2a}^<$, which corresponds to two sequent scattering processes of first order, results as

$$\begin{aligned} W_{2a}^{<(>)}(\omega)&=G_0^{<(>)}(\omega)M^2[G_0(\omega-\overline{\omega})D(\overline{\omega})]^aG_0^a(\omega)M^2[G_0(\omega-\overline{\overline{\omega}})D(\overline{\overline{\omega}})]^aG_0^a(\omega)\\ &+G_0^r(\omega)M^2G_0^{<(>)}(\omega-\overline{\omega})D^{<(>)}(\overline{\omega})G_0^a(\omega)M^2[G_0(\omega-\overline{\overline{\omega}})D(\overline{\overline{\omega}})]^aG_0^a(\omega)\\ &+G_0^r(\omega)M^2[G_0(\omega-\overline{\omega})D(\overline{\omega})]^rG_0^{<(>)}(\omega)M^2[G_0(\omega-\overline{\overline{\omega}})D(\overline{\overline{\omega}})]^aG_0^a(\omega)\\ &+G_0^r(\omega)M^2[G_0(\omega-\overline{\omega})D(\overline{\omega})]^rG_0^r(\omega)M^2G_0^{<(>)}(\omega-\overline{\overline{\omega}})D^{<(>)}(\overline{\overline{\omega}})G_0^a(\omega)\\ &+G_0^r(\omega)M^2[G_0(\omega-\overline{\omega})D(\overline{\omega})]^rG_0^r(\omega)M^2[G_0(\omega-\overline{\overline{\omega}})D(\overline{\overline{\omega}})]^rG_0^{<(>)}(\omega). \end{aligned} \tag{B2}$$

The second diagram corresponds to a two-phonon sequent scattering without crossing of phonon lines. The terms $W_{2b}^{<(>)}$ result in the form

$$W_{2b}^{<(>)}(\omega)=G_0^{<(>)}(\omega)M^2[W_1(\omega-\overline{\omega})D(\overline{\omega})]^a G_0^a(\omega)+G_0^r(\omega)M^2W_1^{<(>)}(\omega-\overline{\omega})D^{<(>)}(\overline{\omega})G_0^a(\omega)$$
$$+G_0^r(\omega)M^2[W_1(\omega-\overline{\omega})D(\overline{\omega})]^r G_0^{<(>)}(\omega), \tag{B3}$$

where the function W_1 is the same as in Eq. (B1). Again the propagator terms $[W_1(\omega-\overline{\omega})D(\overline{\omega})]^{r,a}$ can be found from the correlated parts $W_1^{<(>)}(\omega-\overline{\omega})D^{<(>)}(\overline{\omega})$ by the Hilbert transform (A7).

Finally the third diagram W_{2c} corresponds to a two phonon sequent scattering with crossing of phonon lines. Analytical continuation can be performed as usual,[25] but the mixed structure of indices from crossed lines leads to analytical terms with a more complex structure. In particular it is necessary to introduce propagators for each correlation function separately as follows:

$$-\frac{i}{\hbar}\Theta(1,2)G^{<(>)}(1,2)\equiv G^{<(>)r}(1,2),\quad G^a(1,2)=G^{>a}(1,2)+G^{<a}(1,2),$$

$$\frac{i}{\hbar}\Theta(2,1)G^{<(>)}(1,2)\equiv G^{<(>)a}(1,2),\quad G^r(1,2)=G^{>r}(1,2)+G^{<r}(1,2),$$

$$-\frac{i}{\hbar}\Theta(1,2)D^{<(>)}(1,2)\equiv D^{<(>)r}(1,2),\quad D^a(1,2)=D^{>a}(1,2)-D^{<a}(1,2),$$

$$\frac{i}{\hbar}\Theta(2,1)D^{<(>)}(1,2)\equiv D^{<(>)a}(1,2),\quad D^r(1,2)=D^{>r}(1,2)-D^{<r}(1,2)\,. \tag{B4}$$

Then the correlation part $W_{2c}^{<(>)}$ for the third diagram results in the form

$$W_{2c}^{<(>)}(\omega)=M^4G_0^r(\omega-\overline{\omega_1})D^{<(>)}(\overline{\omega_2})D^{<(>)}(\overline{\omega_1})G_0^a(\omega-\overline{\omega_2})G_0^{<(>)}(\omega-\overline{\omega_1}-\overline{\omega_2})$$
$$-M^4G_0^{<(>)}(\omega-\overline{\omega_1})D^a(\overline{\omega_2})D^r(\overline{\omega_1})G_0^{<(>)}(\omega-\overline{\omega_2})G_0^{>(<)}(\omega-\overline{\omega_1}-\overline{\omega_2})$$
$$+M^4 2\mathrm{Re}\,[G_0^{>r}(\omega-\overline{\omega_1})D^{<r}(\overline{\omega_1})]D^{<(>)}(\overline{\omega_2})G_0^{<(>)}(\omega-\overline{\omega_2})G_0^{<}(\omega-\overline{\omega_1}-\overline{\omega_2})$$
$$+M^4 2\mathrm{Re}\,[G_0^{<r}(\omega-\overline{\omega_1})D^{>r}(\overline{\omega_1})]D^{<(>)}(\overline{\omega_2})G_0^{<(>)}(\omega-\overline{\omega_2})G_0^{>}(\omega-\overline{\omega_1}-\overline{\omega_2})$$
$$+M^4 2\mathrm{Re}\,[G_0^{>r}(\omega-\overline{\omega_1})G^{>r}(\omega-\overline{\omega_1}-\overline{\omega_2})]D^{<(>)}(\overline{\omega_2})D^{>}(\overline{\omega_1})G_0^{<(>)}(\omega-\overline{\omega_2})$$
$$+M^4 2\mathrm{Re}\,[G_0^{<r}(\omega-\overline{\omega_1})G^{<r}(\omega-\overline{\omega_1}-\overline{\omega_2})]D^{<(>)}(\overline{\omega_2})D^{<}(\overline{\omega_1})G_0^{<(>)}(\omega-\overline{\omega_2})$$
$$+M^4 2\mathrm{Re}\,[iG_0^{>r}(\omega-\overline{\omega_1})D^{>r}(\overline{\omega_1})G^{<a}(\omega-\overline{\omega_1}-\overline{\omega_2})]D^{<(>)}(\overline{\omega_2})G_0^{<(>)}(\omega-\overline{\omega_2})$$
$$+M^4 2\mathrm{Re}\,[iG_0^{<r}(\omega-\overline{\omega_1})D^{<r}(\overline{\omega_1})G^{>a}(\omega-\overline{\omega_1}-\overline{\omega_2})]D^{<(>)}(\overline{\omega_2})G_0^{<(>)}(\omega-\overline{\omega_2}). \tag{B5}$$

*Present address: Department of Physics, University of Nottingham, Nottingham NG7 2RD, UK.

[1] V. J. Goldman, D. C. Tsui, and J. E. Cunningham, Phys. Rev. Lett. **36**, 7635 (1987); M. L. Leadbeater *et al.*, Phys. Rev. B **39**, 3438 (1989).

[2] N. S. Wingreen, K. W. Jacobsen, and J. W. Wilkins, Phys. Rev. Lett. **61**, 1396 (1988); Phys. Rev. B **40**, 11 834 (1989).

[3] W. Cai *et al.*, Phys. Rev. Lett. **63**, 418 (1989).

[4] N. Zou and K. A. Chao, Phys. Rev. Lett. **22**, 3224 (1992), and references therein.

[5] L. P. Kadanoff and G. Baym, *Quantum Statistical Mechanics* (Benjamin, New York, 1962).

[6] L. V. Keldysh, Zh. Éksp. Teor. Fiz. 47, 1515 (1964) [Sov. Phys. JETP **20**, 1018 (1965)].

[7] C. Caroli *et al.*, J. Phys. C **5**, 21 (1972).

[8] E. V. Ando and F. Flores, J. Phys.: Condens. Matter **3**, 9087 (1991).

[9] R. Lake and S. Datta, Phys. Rev. B **45**, 6670 (1992).

[10] C. H. Grein, E. Runge, and H. Ehrenreich, Phys. Rev. B **47**, 12 590 (1993).

[11] J. H. Davies, S. Hershfield, P. Hyldgaard, and J. W. Wilkins, Phys. Rev. B **47**, 4603 (1993).

[12] P. Hyldgaard, S. Hershfield, J. H. Davies, and J. W. Wilkins, Ann. Phys. (N.Y.) **236**, 1 (1994).

[13] P. Král, J. Stat. Phys. **86**, 1337 (1997).

[14] S. Hershfield, J. H. Davies, and J. W. Wilkins, Phys. Rev. Lett. **67**, 3720 (1991); Phys. Rev. B **46**, 7046 (1992).

[15] N. S. Wingreen and Y. Meir, Phys. Rev. B **49**, 11 040 (1994), and references therein.

[16] M. H. Hettler and H. Scholler, Phys. Rev. Lett. **74**, 4907 (1995).

[17] H. Shao, D. C. Langreth, and P. Nordlander, Phys. Rev. B **49**, 13 929 (1994); **49**, 13 948 (1994).

[18] G. D. Mahan, *Many Particle Physics* (Plenum, New York, 1981).

[19] G. D. Mahan, Phys. Rev. **145**, 602 (1966).

[20] D. Dunn, Can. J. Phys. **53**, 321 (1975).

[21] R. P. Feynman and A. R. Higgs, *Quantum Mechanics and Path*

Integrals (McGraw-Hill, New York, 1965).
[22] A. B. Migdal, Zh. Éksp. Teor. Fiz. **34**, 1438 (1958).
[23] C. O. Almbladh and P. Minnhagen, Phys. Rev. B **17**, 929 (1978).
[24] R. Balescu, *Lectures in Theoretical Physics* (Interscience Publish., New York, 1961), Vol. III.
[25] D. C. Langreth, in *Linear and Nonlinear Electron Transport in Solids*, edited by J. T. Devresee and E. van Boren (Plenum, New York, 1976).
[26] A. P. Jauho, Phys. Rev. B **32**, 2248 (1985).
[27] J. A. Støevneng *et al.*, Phys. Rev. B **44**, 13 595 (1991).
[28] Y. Meir and N. S. Wingreen, Phys. Rev. Lett. **68**, 2512 (1992).
[29] M. Büttiker, A. Prêtre, and H. Thomas, Phys. Rev. Lett. **70**, 4114 (1993).
[30] C. A. Stafford, Phys. Rev. Lett. **77**, 2770 (1996).
[31] V. Meden, K. Schönhammer, and O. Gunnarson, Phys. Rev. B **50**, 11 179 (1994).
[32] A. A. Abrikosov, L. P. Gorkov, and I. E. Dzyaloshinski, *Quantum Field Theoretical Methods in Statistical Physics*, 2nd ed. (Pergamon, New York, 1965).
[33] F. F. Ouali *et al.*, Phys. Rev. Lett. **75**, 308 (1995).
[34] P. Král, F. W. Sheard, F. F. Ouali, and L. J. Challis (unpublished).
[35] P. Král (unpublished).
[36] P. Král, Phys. Rev. B **53**, 11 034 (1996).
[37] M. P. Anantram and S. Datta, Phys. Rev. B **51**, 7632 (1995).
[38] N. S. Wingreen, A. P. Jauho, and Y. Meir, Phys. Rev. B **48**, 8487 (1993).